UDC 539.4

Effect of Tungsten-Inert-Gas Preheating on Mechanical and Microstructure Properties of Friction Stir Welded Dissimilar Al Alloy and Mild Steel

HanSur Bang,[a] HeeSeon Bang,[a,1] J.-H. Hong,[b] G.-H. Jeon,[b] G.-S. Kim,[b] and A. F. H. Kaplan[c]

[a] Department of Welding and Joining Science Engineering, Chosun University, Gwangju, Republic of Korea

[b] Department of Welding and Joining Science Engineering, Graduate School, Chosun University, Gwangju, Republic of Korea

[c] Department of Engineering Science and Mathematics, Lulea Univversity of Technology, Lulea, Sweden

[1] banghs@chosun.ac.kr

The purpose of this study is to clarify the effect of tungsten-inert-gas (TIG) welding preheating on the mechanical properties of Al6061-T6 and SS400 welded joints by friction stir welding (FSW). FSW joints with and without TIG welding preheating are characterized and compared in terms of their mechanical and microstructural properties. The results show that the TIG assisted hybrid FSW welded joints (TIG-HFSW) provide an enhanced joint strength. The transversal tensile strength of the TIG-HFSW joints exhibited approximately 104% of the Al6061-T6 base metal tensile strength and was higher than that of the FSW joints. Microstructural investigations also reveal that in the HAZ and TMAZ of TIG-HFSW joints, the grains of Al6061-T6 are smaller than those of the FSW welds.

Keywords: dissimilar materials welding, friction stir welding, TIG-assisted hybrid friction stir welding, mechanical and microstructural characteristics.

Introduction. Friction stir welding (FSW) was invented at the Welding Institute of Cambridge University in 1991, is a solid state joining process. Due to its advantages compared with fusion welding methods, friction stir welding serves as a potential welding method for unweldable alloys including nonferrous light materials, such as Al and Mg alloy. As this welding technology utilizes the low temperature process without melting [1–3], it provides not just lower residual stresses, distortion and higher joint strength, but also removes porosity and solidification cracking.

Among nonferrous light materials, Al alloys are widely used in shipbuilding, aerospace, and automotive structures, due to their high specific strength and superior corrosion resistance.

Much research has been conducted to investigate similar and dissimilar FSW joints of this Al alloy [4–7], and Al alloy/Cu, Mg, Ti alloy or Al, Mg alloy/steel [8–10].

However, due to the inadequate joint properties that arise from its considerable plastic deformation, FSW and solid phase welding method has limitations in joining Al alloy and steel. For example, fusion welding methods lead to a formation of a large intermetallic compounds layer, subsequently deteriorating the mechanical properties of joints [11].

Therefore, many researchers have recently aimed to improve joint strength and reduce tool wear through FSW hybrid welding that uses a secondary laser heat source to preheat the steel side [11–16]. One instance is the study conducted by using laser assisted hybrid FSW welding (laser-HFSW) to make butt joints of dissimilar Al6016-T6 aluminum alloy and DC04 mild steel sheet at a thickness of 1 mm [13]. Their solution was to apply the laser assistance when preheating the steel sheet, the laser positioned 10 mm toward the tool and 3 mm toward the butt joint interface. They also found that the specimen welded with a rotation speed of 2000 rpm, a welding feed of 1500 mm/min and a laser power of 1000 W

had the highest tensile shear strength. The highest tensile strength was 200 MPa, which corresponds to about 80% of the tensile strength of an aluminum alloy base material. Likewise, other researchers [15] reported on the mechanical properties of the laser assisted hybrid FSW joint of Al6061-T6 aluminum alloy to SS400 mild steel at a thickness of 3 mm. Their study demonstrated that due to the increased plastic flow and the reduction of welding downward force in joints, the laser HFSW process resulted in a 15–25% improvement in joint strength when compared to that of the FSW joints. Therefore, in order to enhance the joint efficiency and reduce tool wear, this study intends to apply TIG-HFSW, to join Al6061-T6 to SS400.

1. **Experimental Procedures**. The chemical compositions of the aluminum alloy Al6061-T6 and mild steel SS400 are shown below in Table 1. Using FSW and TIG-HFSW, the Al6061-T6 plate was joined to the SS400 plate at a length of 300 mm, a width of 200 mm, and a thickness of 3 mm. Table 2 specifies the joining conditions and Fig. 1 illustrates the schematic diagram of the plates used in FSW and TIG-HFSW. The tool plunge position was kept such that the probe was inserted mainly into the softer material of Al6061-T6 with the probe offset of approximately 0.6 or 1.8 mm towards SS400. The FSW tool material was of 12% Co tungsten carbide (WF20) with a smooth frustum-type probe, which had a shoulder diameter of 18 mm, a probe diameter of 6 mm and a pin length of 2.7 mm. The welding process was carried out with the tool rotating in a counter clockwise (CCW) direction, placing SS400 on the advancing side and Al6061-T6 on the retreating side.

T a b l e 1

Chemical Compositions and Mechanical Properties for Materials Used

Material	Chemical composition (wt.%)								
Al6061-T6	Al	Fe	Si	Cr	Mg	Ti	Cu	Mn	Zn
	98	0.7	0.4–0.8	0.04–0.35	0.1	0.03	0.15–0.4	0.15	0.25
	Mechanical properties								
	Yield strength (MPa)			Elongation (%)			Tensile strength (MPa)		
	300			12			330		
Material	Chemical composition (wt.%)								
SS400	C	Si	Mn	P	S	Ni	Cr	Mo	
	0.16	0.32	1.63	0.008	0.013	0.03	0.04	–	
	Mechanical properties								
	Yield strength (MPa)			Elongation (%)			Tensile strength (MPa)		
	330			37			450		

T a b l e 2

Welding Condition for TIG-HFSW

Parameter	Tool rotation speed (rpm)	Axial load (kgf)	Traveling speed (mm/min)	TIG current (A)	Pin offset (mm)
Value	400	300	48	60	0.6, 1.8

In the TIG-HFSW method, the TIG welding torch used to preheat SS400 was placed approximately 20 mm in front of FSW tool, inclined at 60°.

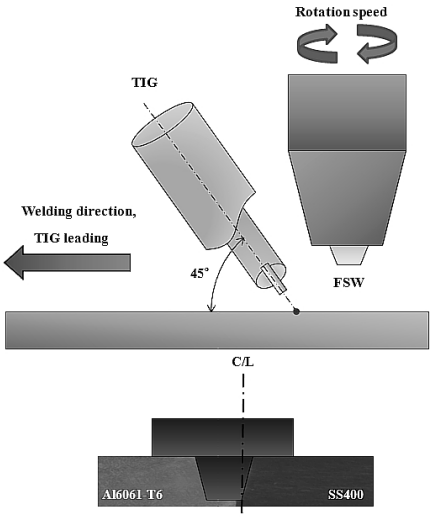

Fig. 1. Schematic diagram of the FSW and TIG-HFSW.

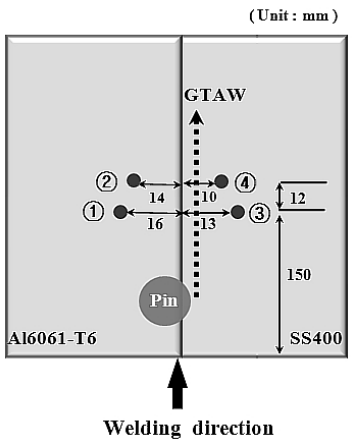

Fig. 2. Temperature measurement points in the workpiece.

In order to specify the effect of the TIG heat source, temperature histories of the FSW and TIG-FSW joints, measured through type K thermocouples, were compared. Figure 2 shows the temperature measurement points in the workpiece.

While the Vickers hardness test and tensile test evaluated the mechanical properties of the joints, the optical microscopy and scanning electron microscopy (SEM) equipped with an X-ray energy dispersive spectroscopy (EDS) examined their metallurgical characteristics.

2. **Results and Discussion**. Figure 3 shows the tensile strength of the FSW and TIG-HFSW joints in different probe offsets of 0.6 and 1.8 mm. It reveals that due to the plastic deformation in tool rotation and fracture at the hard material steel side, the tensile strength of the FSW and TIG-HFSW joints increased in the probe offset of 0.8 mm. Under the same welding condition, the maximum tensile strength of the TIG-HFSW joints was higher than that of the FSW joints, respectively measured to be 344 and 191 MPa at the 0.6 mm probe offset. While the highest tensile strength of the TIG-HFSW joints was about 344 MPa at a 0.6 mm probe offset, which is 104% of that of the Al6061-T6 base metal, the highest tensile strength obtained for the FSW joints was about 191 MPa, which is 56% of that of the Al6061-T6 base metal.

Furthermore, the elongation to the fracture of the TIG-HFSW joints sharply increased to 1.2%, which is approximately 1.5 times that of the FSW joints. These results confirm that an elongation in the TIG-HFSW joints can increase significantly through a sufficient material flow and the partial annealing effect of a secondary TIG heat source. Thus, there seems to be a strong correlation between the preheating of the SS400 side and an improvement in joint strength. The tensile testing of the FSW joints also demonstrated that a crack initiation tends to occur at the lower part of a joint where welding is not entirely achieved. In fact, the fracture path of the FSW joints was along the interface between the Al6061-T6 and SS400 while the fracture path of the TIG-HFSW joints was along the interface between the Al6061-T6 and SS400 steel fragments.

Figure 4 shows the macroscopic overview of the surface and cross-section in the FSW joints (a) and the TIG-HFSW joints (b) in different probe offsets of 0.6 and 1.8 mm. Decreasing the probe position with a probe offset of 0.6mm induced more material flow between dissimilar materials without breaking the FSW tool. It thus confirmed that a secondary heat source TIG to SS400 allows for more material flow between dissimilar materials in the TIG-HFSW joints than in FSW joints.

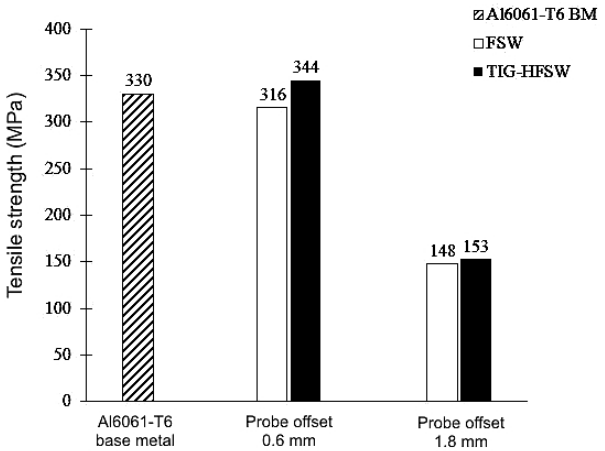

Fig. 3. Tensile test results of FSW and TIG-HFSW joints with probe offsets.

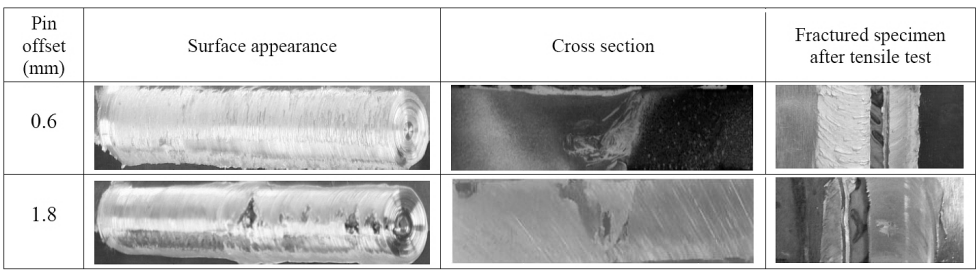

a

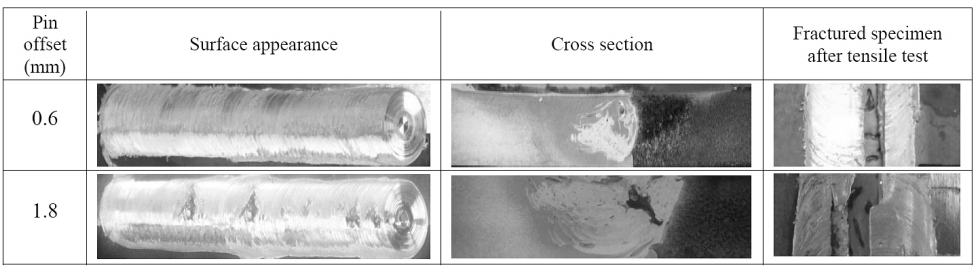

b

Fig. 4. Macro observation of FSW (a) and TIG-HFSW (b) joints with probe offsets.

In the FSW joints, in different probe offsets of 0.6 and 1.8 mm, the specimens were not welded at the bottom area of the plate thickness. It can be inferred that this was due to a material flow shortage that resulted from an insufficient heat generation and a high difference in melting points between dissimilar materials. In the TIG-HFSW joints, on the other hand, the specimens were fully welded in the probe offsets of 0.6 mm. In fact, the specimens revealed joints that were non-welded at the bottom area of plate thickness in the probe offsets of 1.8 mm, as shown by the arrow in the cross section. Furthermore, it was found that minute steel fragments at the retreating side scattered away from SS400 because of the considerable stirring effect of the tool probe in SZ.

Figure 5 compares the temperature histories measured through the thermocouple in the FSW and TIG-HFSW joints in probe offsets of 0.6 mm; (a) is the Al6061-T6 side and

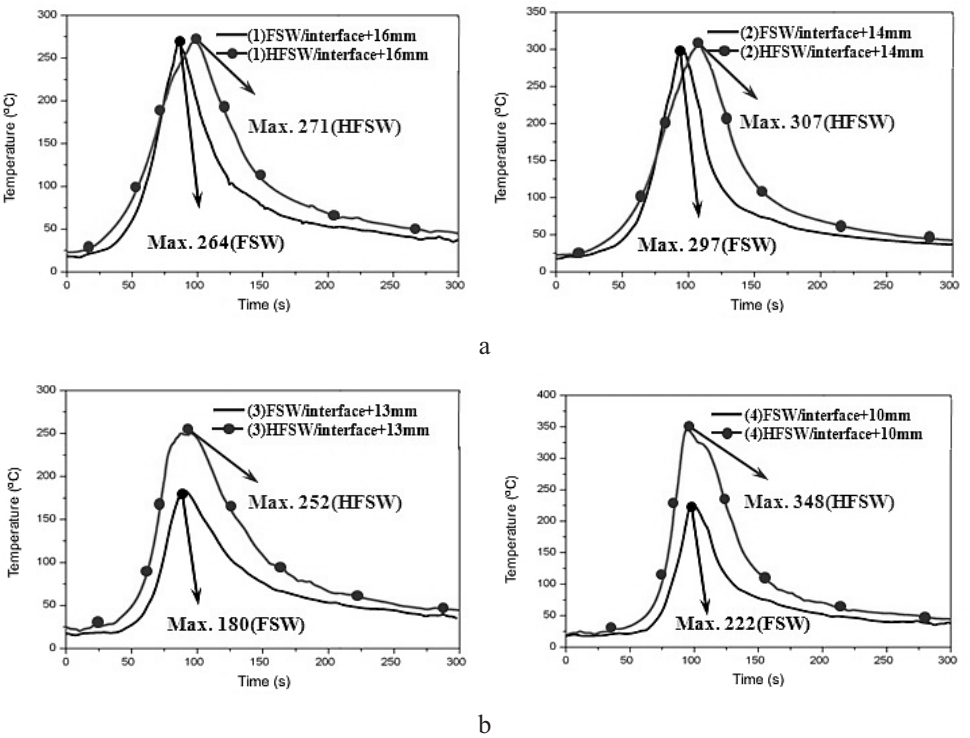

Fig. 5. Temperature histories measured through the thermocouple in FSW and TIG-HFSW joints: (a) Al6061-T6 side; (b) SS400 side.

(b) is the SS400 side. As shown in Fig. 5, the maximum temperature of the TIG-HFSW joints was higher than that of the FSW joints. The difference in the maximum temperatures on the SS400 side between the FSW and TIG-HFSW joints was considerably large at approximately 80–126℃, whereas it was smaller on the Al6061-T6 side, at approximately 7–10℃.

Figure 6 shows the optical microstructure of the FSW and TIG-HFSW joints in probe offset of 1.2 mm; (a) is the FSW joints and (b) is the TIG-HFSW joints. As Fig. 6a illustrates, the microstructure of Al6061-T6 at the retreating side in the heat affected zone (HAZ) showed a slightly larger than that of the Al6061-T6 base metal. On the other hand, the grains of Al6061-T6 at the retreating side in the thermally-mechanically affected zone (TMAZ) were slightly fine, due to the mechanical welding force and the friction heat caused by FSW tool shoulder.

The weld nugget had fine dynamic recrystallized grains of Al6061-T6 and the fine steel fragments that had scattered away from the SS400. It also showed a partially unwelded zone in the bottom of interface between Al6061-T6 and SS400, due to the lack of a plastic flow behavior. In contrast, as shown in the Fig. 6b, in the TIG-HFSW joints, the grains of Al6061-T6 at the retreating side were finer than those of the FSW joints in the HAZ and TMAZ. The weld nugget had a composite structure of finer recrystallized grains of Al6061-T6 and small steel particles that had scattered away from the SS400. Furthermore, it showed a fully welded zone in the bottom of interface between Al6061-T6 and SS400, as there was a sufficient and smooth plastic flow phenomenon, unlike in the FSW joints. The finer dynamic recrystallized grains in the SZ can be considered since the significant plastic deformation results from an increased material flow by using TIG as a preheating source to SS400.

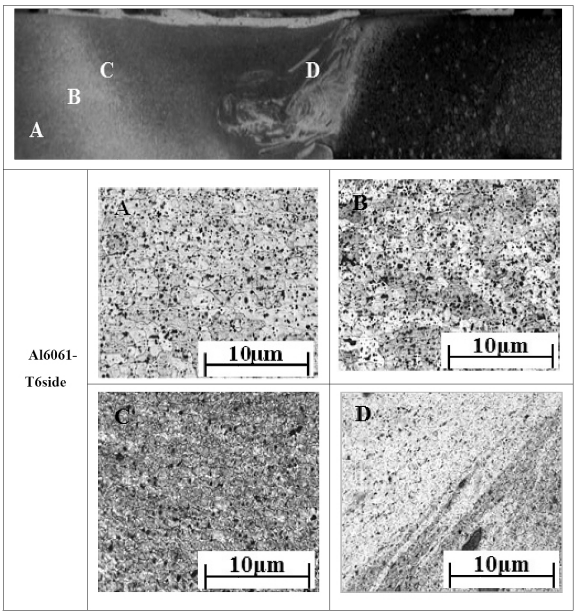

a

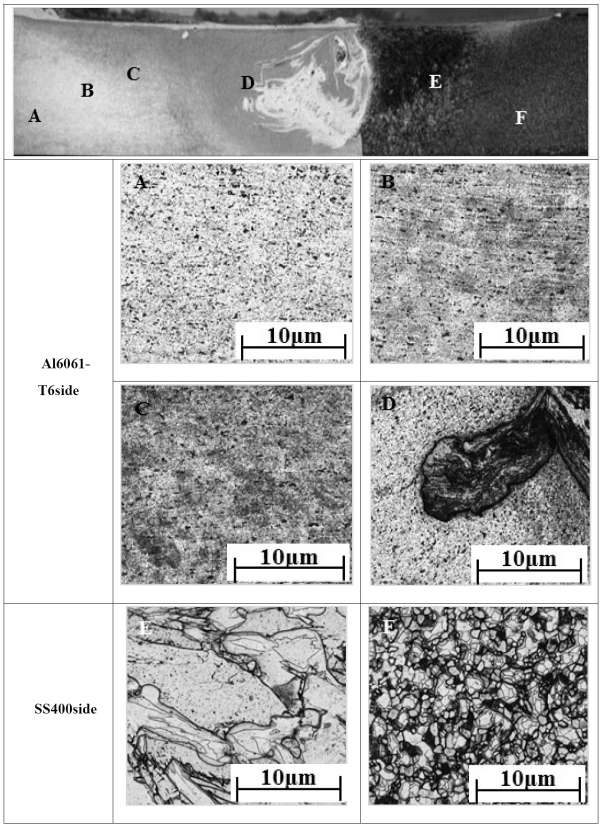

b

Fig. 6. Optical microscope of FSW (a) and TIG-HFSW (b) joints: (*A*) Al6061-T6 base metal, (*B*) HAZ in the Al6061-T6, (*C*) TMAZ in the Al6061-T6, (*D*) SZ in the Al6061-T6, (*E*) HAZ and TMAZ in the SS400 side, and (*F*) SS400 side base metal.

Figure 7 illustrates the SEM-EDS analysis of the weld nugget of the TIG-HFSW joints; (a) is the weld nugget zone along Al6061-T6 at the retreating side while (b) is the weld nugget zone along SS400 at the advancing side. As shown in Fig. 7a, the chemical compositions of points 1, 2, and 3 were 0.56%Fe-99.44%Al, 0.62%Fe-99.38%Al, and 96.83%Fe-3.17%Al (at.%), respectively. Points 1 and 2 had the same chemical composition as the original Al6061-T6, whereas point 3 had the same chemical composition as the original SS400. According to this phase diagram, point 3 is a brittle intermetallic compound of FeAl or $FeAl_3$, which has the tendency to decrease joint strength. As shown in Fig. 7b, the chemical compositions of points 1, 2, and 3 were 99.16%Fe-0.84Al, 99.74%Fe-0.26Al, and 99.44%Fe-0.56Al (at.%), respectively. Only the points 1, 2, and 3 found SS400 compositions along the SS400 side. The image also deduces the region where Al6061-T6 did not diffuse.

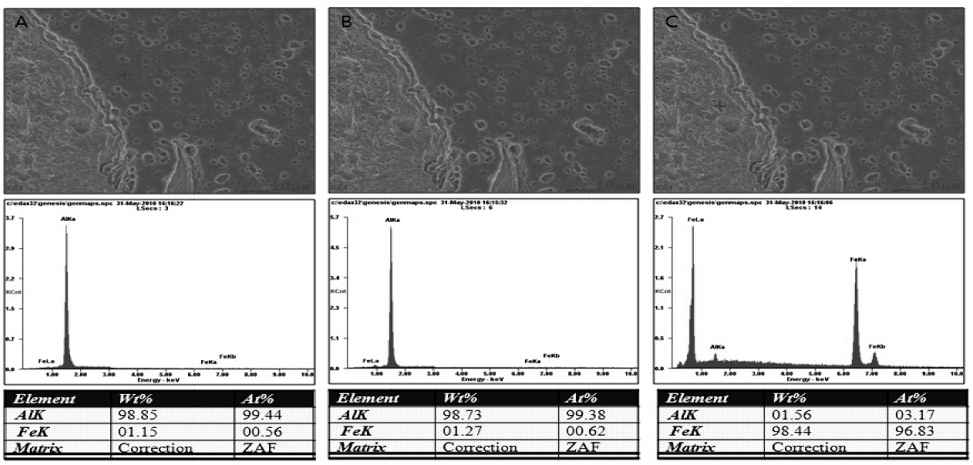

Element	Wt%	At%
AlK	98.85	99.44
FeK	01.15	00.56
Matrix	Correction	ZAF

Element	Wt%	At%
AlK	98.73	99.38
FeK	01.27	00.62
Matrix	Correction	ZAF

Element	Wt%	At%
AlK	01.56	03.17
FeK	98.44	96.83
Matrix	Correction	ZAF

a

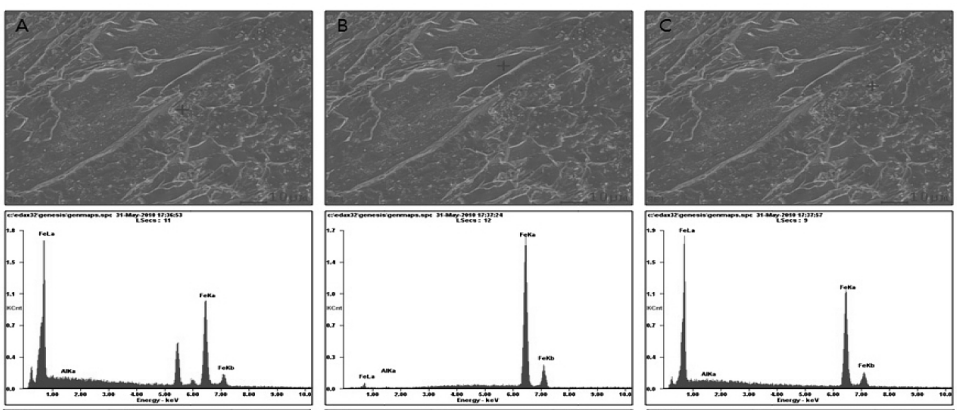

Element	Wt%	At%
AlK	00.41	00.84
FeK	99.59	99.16
Matrix	Correction	ZAF

Element	Wt%	At%
AlK	00.13	00.26
FeK	99.87	99.74
Matrix	Correction	ZAF

Element	Wt%	At%
AlK	00.27	00.56
FeK	99.73	99.44
Matrix	Correction	ZAF

b

Fig. 7. SEM image and EDS analysis of TIG-HFSW joints: (a) Al6061-T6 joints; (b) SS400 joints.

Conclusions. The TIG-HFSW technique was successfully adopted to join Al6061-T6 to SS400. In addition, the tensile strength and the microstructure of joints were examined. The results are summarized as follows:

1. While the highest tensile strength was approximately 104% when joined with TIG-FSW, the highest tensile strength of joints by FSW was found to be approximately 56% of that of the Al6061-T6 base metal. This increase in the TIG-FSW joints can be attributed to the sufficient materials stirring and the partial annealing effect of dissimilar materials in TIG preheating.

2. The temperature history measured in the FSW and TIG-HFSW joints shows that the difference in maximum temperatures between the FSW and TIG-HFSW joints in the SS400 side was approximately 80–126℃, whereas it was approximately 7–10℃ in the Al6061-T6 side.

3. In the HAZ and TMAZ of TIG-HFSW joints, the grains of Al6061-T6 were finer than those of the FSW joints. Due to the sufficient and smooth plastic flow phenomena unlike that of the FSW, the weld nugget of the TIG-HFSW joints exhibited a fully welded zone in the bottom area of the interface between Al6061-T6 and SS400. The smaller dynamic recrystallized grains in the SZ can be thus due to the generation of significant plastic deformation.

Acknowledgments. This work was supported by the Industrial Technology Innovation Program (10049005) funded By the Ministry of Trade, Industry and Energy (MI, Korea).

1. K. Chen, W. Gan, K. Okamoto, et al., "The mechanism of grain coarsening in friction-stir welded AA5083 after heat treatment," *Metall. Mater. Trans. A*, **42**, 488–507 (2011).
2. E. Cerri and P. Leo, "Warm and room temperature deformation of friction stir welded thin aluminium sheets," *Mater. Des*., **31**, 1392–1402 (2010).
3. W. Yuan, R. S. Mishra, S. Webb, et al., "Effect of tool design and process parameters on properties of Al Alloy 6016 friction stir spot welds," *J. Mater. Proc. Tech*., **211**, 972–977 (2011).
4. I. Shigematsu, Y. J. Kwon, K. Suzuki, et al., "Joining of 5083 and 6061 aluminum alloys by friction stir welding," *J. Mater. Sci. Lett.*, **22**, 353–356 (2003).
5. J. J. S. Dilip, M. Koilraj, V. Sundareswaren, et al., "Microstructural characterization of dissimilar friction stir welds between AA2219 and AA5083," *Trans. Indian Inst. Metals*, **63**, 757–764 (2010).
6. M. Ghosh, K. Kumar, S. V. Kailas, and A. K. Ray, "Optimization of friction stir welding parameters for dissimilar aluminum alloys," *Mater. Des.*, **31**, 3033–3037 (2010).
7. Ch. Y. Lee, W. B. Lee, J. W. Kim, et al., "Lap joint properties of FSWed dissimilar formed 5052 Al and 6061 Al alloys with different thickness," *J. Mater. Sci*., **43**, 3296–3304 (2008).
8. Y. C. Chen and K. Nakata, "Microstructural characterization and mechanical properties in friction stir welding of aluminum and titanium dissimilar alloys," *Mater. Des*., **30**, 469–474 (2009).
9. Y. C. Chen and K. Nakata, "Effect of tool geometry on microstructure and mechanical properties of friction stir lap welded magnesium alloy and steel," *Mater. Des.*, **30**, 3913–3919 (2009).
10. T. Saeid, A. Abdollah-Zadeh, and B. Sazgari, "Weldability and mechanical properties of dissimilar aluminum–copper lap joints made by friction stir welding," *J. Alloys Compd*, **490**, 652–655 (2010).
11. Y. C. Chen and K. Nakata, "Effect of the surface state of steel on the microstructure and mechanical properties of dissimilar metal lap joints of aluminum and steel by friction stir welding," *Metal. Mater. Trans. A*, **39**, 1985–1992 (2008).

12. M. Movahedi, A. H. Kokabi, S. M Seyed Reihani, and H. Najafi, "Mechanical and microstructural characterization of Al-5083/St-12 lap joints made by friction stir welding," *Proc. Eng.*, **10**, 3297–3303 (2011).
13. M. Merklein and A. Giera, "Laser assisted friction stir welding of drawable steel-aluminium tailored hybrids," *Int. J. Mater. Form.*, **1**, 1299–1302 (2008).
14. C. M. Chen and R. Kovacevic, "Joining of Al 6061 to AISI 1018 steel by combined effects of fusion and solid state welding," *Int. J. Mach. Tools Manuf.*, **44**, 1205–1214 (2004).
15. H. S. Bang, H. S. Bang, and G. H. Jeon, "A study on weldability and mechanical characteristics of dissimilar materials butt joints by laser assisted friction stir welding," *J. Korean Weld. Join. Soc.*, **28**, 678–683 (2010).
16. D. K. Yaduwanshi, S. Bag, and S. Pal, "Effect of preheating in hybrid friction stir welding of aluminum alloy," *J. Mater. Eng. Perform.*, **23**, 3794–3803 (2014).

Received 03. 08. 2015